Clicked BODIPY-Fullerene-Peptide Assemblies: Studies of Electron Transfer Processes in Self-Assembled Monolayers on Gold Surfaces

Jad Rabah, Houssein Nasrallah, Karen Wright, Isabelle Gérard, Hélène Fensterbank, Thi Tuyet Van Bui, Jérôme Marrot, Thu-Trang Tran, Anam Fatima, Minh-Huong Ha-Thi, et al.

Clicked BODIPY-Fullerene-Peptide Assemblies: Studies of Electron Transfer Processes in Self-Assembled Monolayers on Gold Surfaces

Jad Rabah,[a] Houssein Nasrallah,[a] Karen Wright,[a] Isabelle Gérard,[a] Hélène Fensterbank,[a] Thi-Tuyet-Van Bui,[a] Jérôme Marrot,[a] Thu-Trang Tran,[b] Anam Fatima,[b] Minh-Huong Ha-Thi,[b] Rachel Méallet,[b] Gotard Burdzinski,[c] Gilles Clavier,[d] Souhir Boujday[e] Hubert Cachet,[f] Catherine Debiemme-Chouvy,[f] Emmanuel Maisonhaute,[f*] Anne Vallée, [*a,e] and Emmanuel Allard*[a]

[a] Université Paris-Saclay, UVSQ, CNRS, Institut Lavoisier de Versailles, 78000, Versailles, France, e-mail: anne.vallee@uvsq.fr; emmanuel.allard@uvsq.fr

[b] Université Paris-Saclay, CNRS, Institut des Sciences Moléculaires d'Orsay, 91405, Orsay, France.

[c] Adam Mickiewicz University, Poznan, Faculty of Physics, PL-61614 Poznan, Poland

[d] Université Paris-Saclay, ENS Paris-Saclay, CNRS, PPSM, 91190 Gif-sur-Yvette, France.

[e] Sorbonne Université, CNRS, Laboratoire de Réactivité de Surface (LRS), 4 place Jussieu, F-75005 Paris, France.

[f] Laboratoire Interfaces et Systèmes Electrochimiques, Sorbonne Université, CNRS, 4 place Jussieu, 75005 Paris, France, e-mail: emmanuel.maisonhaute@upmc.fr

Abstract – Two BODIPY-C_{60}-peptide assemblies were synthesized by CuAAC reactions of BODIPY-C_{60} dyads and a helical peptide functionalized with a terminal alkyne group and an azide group, respectively. The helical peptide within these assemblies was functionalized at its other end by a disulfide group, allowing formation of self-assembled monolayers (SAMs) on gold surfaces. Characterizations of these SAMs, as well as those of reference molecules (BODIPY-C_{60}-alkyl, C_{60}-peptide and BODIPY-peptide), were carried out by PM-IRRAS and cyclic voltammetry. BODIPY-C_{60}-peptide SAMs are more densely packed than BODIPY-C_{60}-alkyl and BODIPY-peptide based SAMs. These findings were attributed to the rigid peptide helical conformation along with peptide-peptide and C_{60}-C_{60} interactions within the

monolayers. However, less dense monolayers were obtained with the target assemblies compared to the C_{60}-peptide, as the BODIPY entity likely disrupts organization within the monolayers. Finally, electron transfer kinetics measurements by ultra-fast electrochemistry experiments demonstrated that the helical peptide is a better electron mediator in comparison to alkyl chains. This property was exploited along with those of the BODIPY-C_{60} dyads in a photo-current generation experiment by converting the resulting excited and/or charge separated states from photo-illumination of the dyad into electrical energy**.**

Introduction

Proteins play a major role in electron transfer (ET) processes in natural systems, perhaps most importantly in photosynthesis. Over the recent years, researchers have sought to mimic these processes artificially on a smaller scale, by using simple model peptides to replace proteins for electron transport.[1]

Many studies used α-helical peptides for this purpose, as this secondary structure presents significant advantages over other conformations such as β-sheets. Stable α-helices may be formed by relatively few amino acids and they can be easily functionalized, either at the peptide termini, or on the side chain groups along the peptide sequence. Anchoring moieties can be introduced to allow attachment to surfaces, for example thiol or disulfide groups for grafting on gold surfaces. These immobilization processes may lead to the formation of densely packed and structurally ordered self-assembled monolayers (SAMs). Additional grafting of a redox entity, most commonly ferrocene (Fc), to the opposite peptide terminus, has allowed studies of ET processes across peptides using electrochemistry experiments.[1] From these studies, it was clearly demonstrated that helical peptides are good electron mediators, able to promote ET over long distances.[2] In addition, the ET was more efficient along the direction of the dipole moment of the peptide than in the opposite direction.[3] Taken together, these features of α-helical peptides make them promising molecules for integration into (bio)electronic systems.[4] The unusual ET properties displayed by self-assembled monolayers of helical peptides covalently linked to gold surfaces have recently been exploited in applications related to solar energy conversion.[5] Helical peptides were functionalized either at one of their termini or along the peptide chain by different chromophores,[6] which acted as electron donors or electron acceptors in their photo-excited states. One striking feature of α-helical peptide SAMs, in addition to their ET properties, is that the rigidity of the helices keeps the chromophores away from the metallic surface and thus restricts quenching of the chromophore excited state, which

is a limiting factor in photocurrent generation.[7] Photocurrent generation by such peptide-based SAMs, using an aqueous solution of sacrificial electron donor (anodic current) or electron acceptor (cathodic current) has been clearly established, demonstrating that these systems can be viewed as artificial mimics of natural photosynthesis. However, these systems were exclusively developed with sensitizer substituted helical peptides in which the sensitizer displayed light-harvesting properties only in the UV region, except in the case of porphyrins.[6f-i]

In this context, we propose to expand the scope of peptide-based self-assembled monolayers in photo-induced current generation by adding a donor-acceptor dyad to one of the peptide termini. These dyads, which give rise to electron transfer and/or energy transfer thanks to the photoexcitation of either the donor or acceptor moiety, are of primary importance in applications related to solar energy conversion.[8] We believe that these intramolecular photo-induced processes could be exploited in the development of new peptide-based SAMs in energy-harvesting devices. The immobilization of donor-acceptor dyads on surfaces has already been described in the literature for such applications, but never with helical peptides to our knowledge.[7, 9] We have recently developed such donor-acceptor dyads composed of a BODIPY (BDP) donor and a Fullerene (C_{60}) unit (see Scheme 1). While BDP donors display remarkable light harvesting properties in the visible region, C_{60} has exceptional properties both as an electron acceptor and also low reorganization energies in ET reactions. In all these dyads, rapid photo-induced electron and photo-induced energy transfer processes from BDP to C_{60} were clearly demonstrated, leading to a charge separated state and a triplet excited state localized on C_{60}, respectively.[10] Both states could be involved in photo-current generation. In addition, from a synthetic point of view, our strategy using clickable fullerene building blocks allowed the design of BDP-C_{60} conjugates bearing a chemical functionality available for further derivatization with complex structures, here the helical peptide. This approach to the construction of complex architectures that integrate Fullerene C_{60} allows successful syntheses of systems that would be difficult to obtain by other methods, for example by direct functionalization of the C_{60} core.

In this article, we report the synthesis and characterization of two sophisticated BPD-C_{60}-peptide assemblies from two BDP-C_{60} dyads and a hexapeptide, all these precursors being previously described by our group.[10a, 11] The BDP-C_{60} dyads, which differ only by the nature of the linker that associates the BDP and C_{60}, are functionalized by a free or protected alkyne. As for the peptide unit, we used a simple hexapeptide containing a repeating sequence of α-aminoisobutyric acid (Aib) and two L-alanine (Ala) residues, $(Aib\text{-}Ala\text{-}Ala)_2$.[11a] This

composition and the position of the Aib residues in the peptide are extremely important since they promote the formation of a helical structure. In addition, the peptide sequence is very short in order to promote efficient and fast ET to the metal surface, as the ET rate decreases with the distance between the metallic surface and the electroactive unit. [12]The hexapeptide was functionalized at its *N*-terminus by a disulfide group, which acts as a bidentate ligand for the gold surface and at its *C*-terminus by an azide group, allowing grafting of the BDP-C_{60} dyads via a Copper-catalyzed Alkyne-Azide Cycloaddition (CuAAC) reaction. We also synthesized disulfide substituted reference molecules in order to demonstrate the benefit provided by each entity (peptide, BDP and C_{60}) in photocurrent generation processes. The BDP-C_{60}-peptide assemblies and reference molecules were immobilized on a gold surface, and the resulting SAMs were characterized using surface characterization and electrochemical techniques. Finally, the combination of ultra-fast electrochemistry and photo-current generation experiments also allowed us to study electron transfer processes in these immobilized systems.

Results and Discussion

Synthesis. The chemical structures of the two target BDP-C_{60}-peptides (**6** and **8**), precursors (**4** and **5**) and reference molecules (**7**, **9**, **10** and **11**) are depicted in Figure 1. BDP-C_{60} assemblies containing a peptide (**6** and **8**) or an alkyl chain (**7**) were obtained using our previously reported strategies based on click chemistry.[11, 13] These sophisticated assemblies have been prepared in a simple manner by post-functionalization of clickable fullerene building blocks that bear two different reactive centers. The synthetic procedure for the preparation of these derivatives is presented in Scheme 1. We used two BDP-C_{60} dyads **1** and **2**, recently described by our group, that carry a free or protected alkyne moiety, respectively.[10a, 11b] The first target BDP-C_{60}-peptide **6** was synthesized by reacting the corresponding BDP-C_{60} **1** precursor with the azido-hexapeptide **4** under our previously reported CuAAC conditions, using a preformed complex [Cu(I)ligand(hexabenzyltren]Br in dichloromethane (DCM), prepared from CuBr and (hexabenzyl)tren ligand.[11a] BDP-C_{60}-peptide **6** was isolated after chromatographic separation using silica gel then gel permeation in 67 % yield. Likewise, the reaction of **1** with an azido-alkyl derivative **5** provided the corresponding reference BDP-C_{60}-alkyl **7** in 75 % yield. The second target BDP-C_{60}-peptide **8** was obtained in a two-step one pot approach.[11b] The corresponding BDP-C_{60} dyad **2** precursor bearing a protected alkyne was first deprotected using TBAF in DCM, followed by the addition of the peptide **4** in the presence of

10.1002/cplu.202300717

[Cu(I)ligand(hexabenzyl)tren]Br complex. The desired target molecule **8** was isolated using the same procedure as **6** in 39 % yield. Finally, the reference derivative BDP-peptide **9** was synthesized and isolated in a 98 % yield by reacting the corresponding BDP-alkyne **3** precursor[13a] with the azido-hexapeptide **4** under the same conditions as mentioned above. Despite the structural complexity of this family of molecules, all the derivatives were isolated in good to excellent yields after purification by column chromatography (*vide supra*).

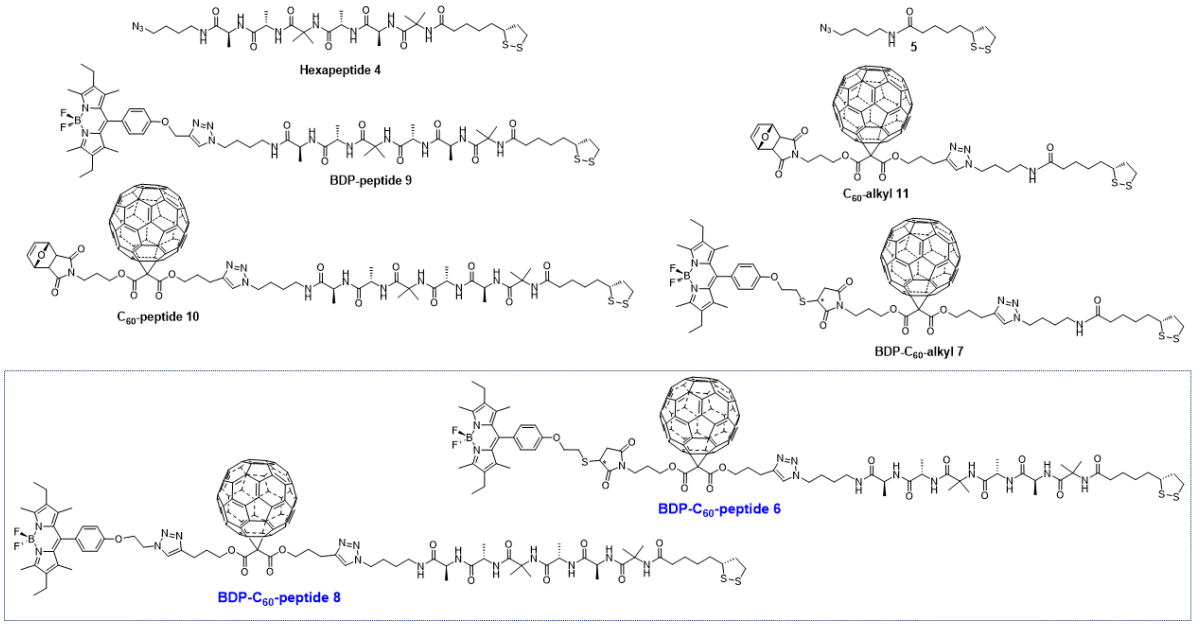

Figure 1. Chemical structures of target BDP-C_{60}-peptides **6** and **8,** and reference molecules (**4, 5, 7, 9** and **10-11**).

10.1002/cplu.202300717

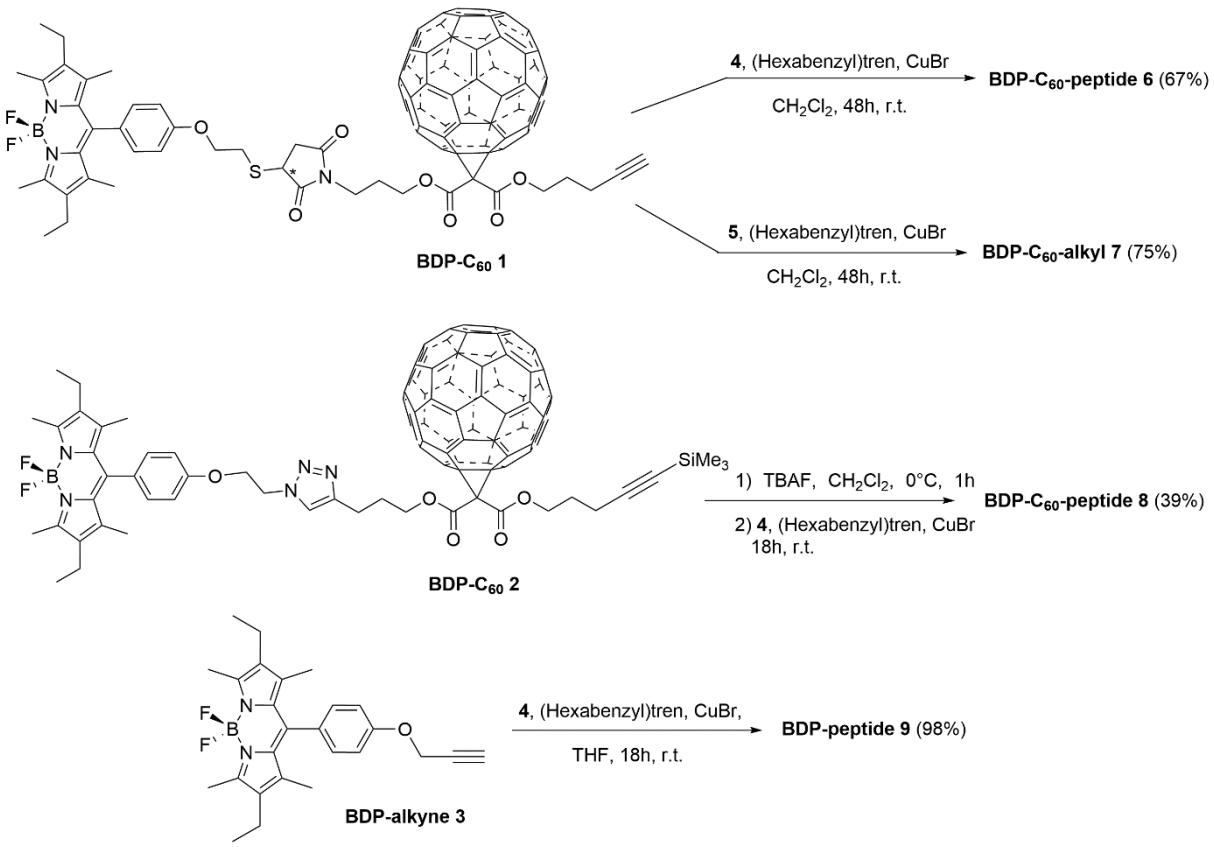

Scheme 1. Synthesis strategies of target BDP-C_{60}-peptides **6** and **8**, and reference molecules **7** and **9**.

Characterization. All the new compounds were characterized by NMR spectroscopy and mass spectrometry. The corresponding data in addition to the complete assignment of the signals are provided in the experimental section (see supporting materials, Figures S3-S33).

^{1}H NMR studies. The proton NMR analyses of the reference and target assemblies were conducted in the first place in $CDCl_3$. The obtained spectra allowed the identification of the proton resonances, except those belonging to the amide protons of the peptide-based assemblies; as some were too close to allow a complete assignment of the signals. Therefore, we decided to perform the analyses in deuterated pyridine C_5D_5N since it is well-known that the amide protons are well-defined and dispersed in this solvent allowing a proper and complete attribution of the assemblies containing peptide chains.[11a] The ^{1}H NMR spectra of the target molecules **6** and **8** are displayed in Figures 2a and 2b. These spectra show characteristic signals of all three components of the assemblies, in addition to the typical singlet of the triazole unit (denoted H_a) that confirms the grafting of the helical peptide on the dyads.

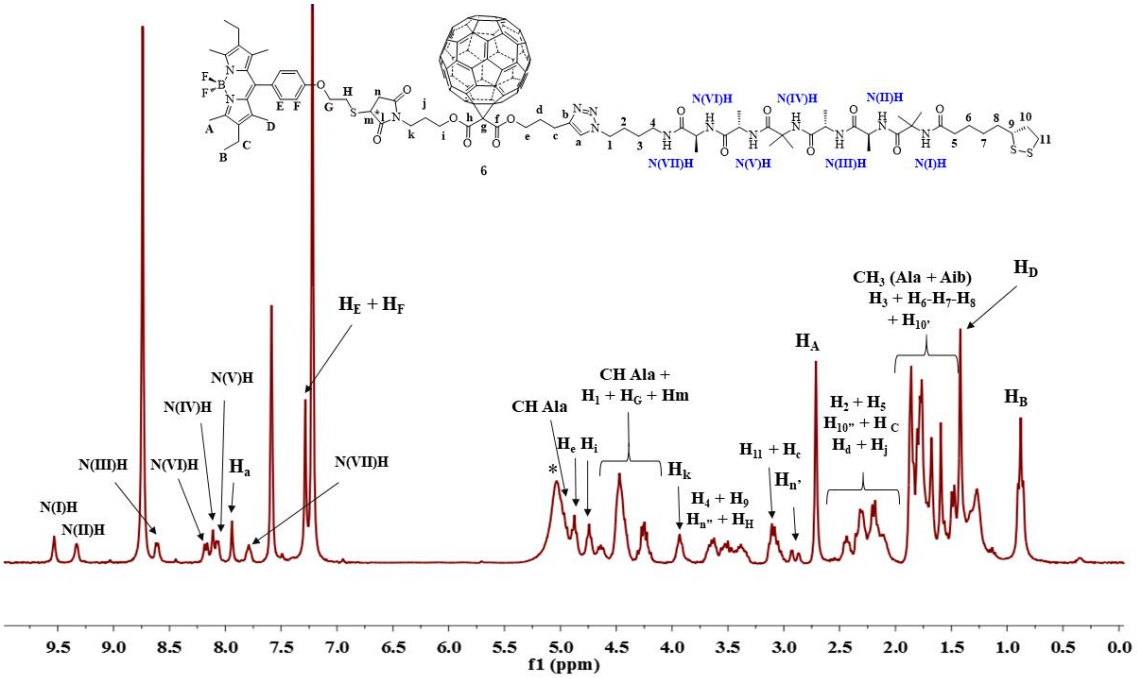

Figure 2a. ^{1}H NMR spectrum in C_5D_5N (300 MHz, 298 K) of the target BDP-C_{60}-peptide **6**. The peak labeled with an asterisk is due to residual water.

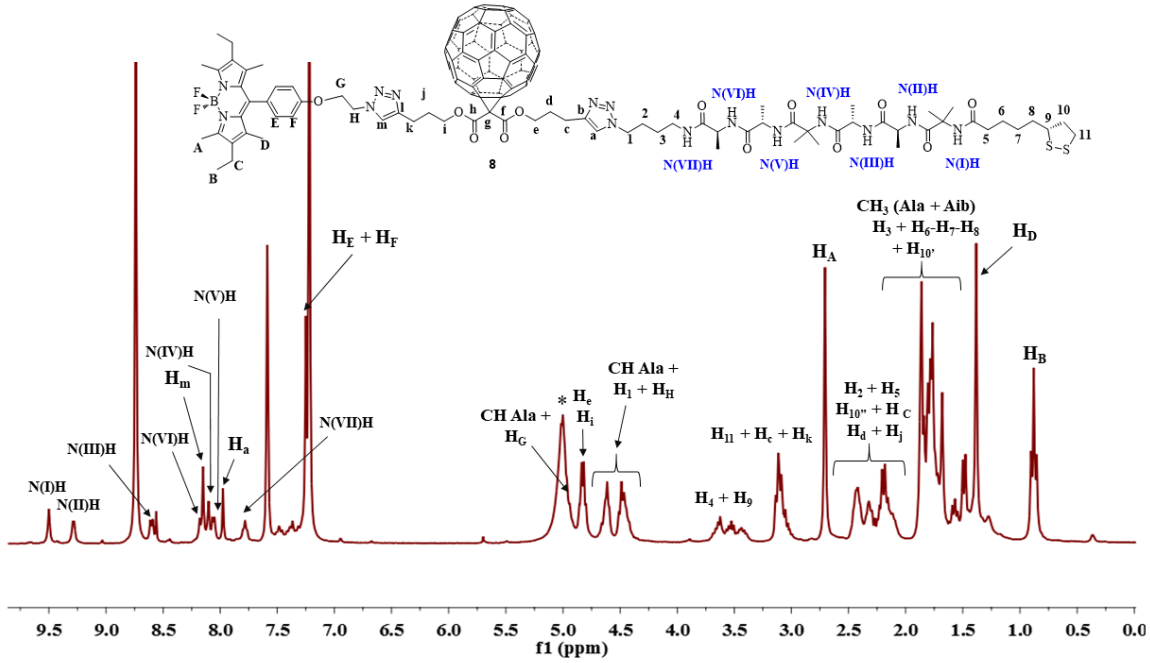

Figure 2b. ^{1}H NMR spectrum in C_5D_5N (300 MHz, 298 K) of the target BDP-C_{60}-peptide **8**. The peak labeled with an asterisk is due to residual water.

Peptide conformational properties. The conformational properties of the reference peptide **4** and C_{60}-peptide **10** were previously reported in solution using a combination of FT-IR, circular dichroism (CD) and ^{1}H NMR analyses. From these measurements, it was clearly demonstrated that the peptide in these derivatives adopts a helical conformation in both $CDCl_3$ and MeOH

solutions and that this conformation is not modified by the presence of the C_{60} unit.[11a, 14] It seems likely that we have the same trend in the BDP-C_{60}-peptide **6** and **8** since the BDP is connected on one side of the C_{60} while the peptide with its helical conformation is located on the other side.

Moreover, previous NMR experiments suggest that our peptide probably adopts a 3_{10}-helical conformation in $CDCl_3$ solution.[11a] However, an α-helical conformation preference has not been fully ruled out in these derivatives since the 3_{10}-/α-helix conformational equilibrium and interconversion has already been noticed in some cases of Aib- and Ala-rich short peptides.[15] Single crystals of a precursor of the peptide **4**, with a BOC group instead of lipoic acid group, suitable for X-ray diffraction were obtained by slow evaporation from a CH_2Cl_2/Et_2O solution. The X-ray structure is composed of one peptide molecule and two co-crystallized $CHCl_3$ molecules (Figure 3).[16] The structure unambiguously confirms the adoption of a helical conformation. A closer inspection of the intramolecular hydrogen bonding and the torsion angles (ω, Φ and Ψ) allowed a better understanding of the peptide conformation. The peptide backbone is folded with a first i, i+3 C=O···H-N hydrogen bond at the *N*-terminal followed by three i, i+4 C=O···H-N hydrogen bonds. This pattern is consistent with an α-helix conformation, modified by a tighter turn (3_{10}-helix) at the *N*-terminal. This type of conformation has previously been observed in other peptide and protein sequences.[15d] The extracted geometrical parameters are listed in Table 1.

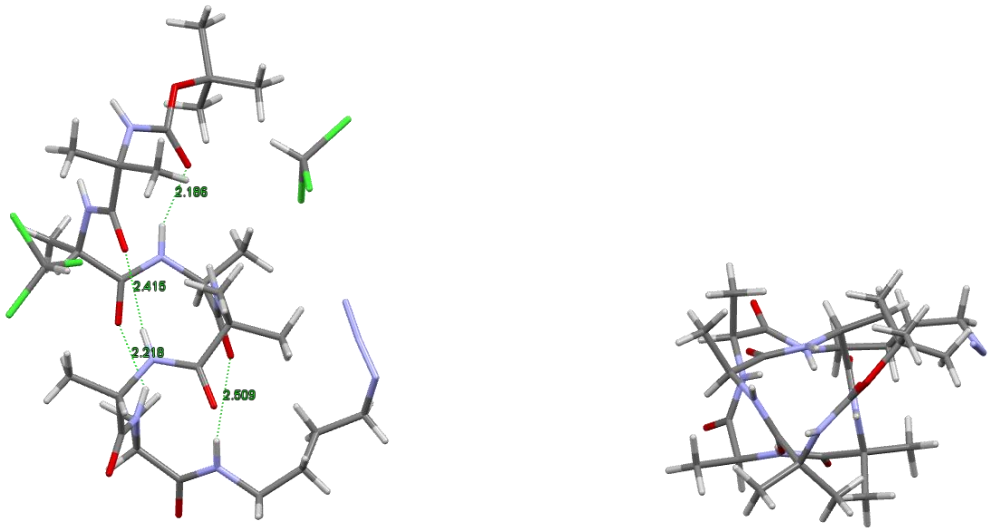

Figure 3. X-ray diffraction structure of a precursor of hexapeptide **4**. Intramolecular H-bonds are represented by green dashed lines.

Table 1. Summary of the extracted torsion angles (Φ, Ψ and ω) of a precursor of hexapeptide **4**.

Residues	Φ	Ψ	ω
1	-56	-40	-176
2	-58	-31	180
3	-63	-45	179
4	-56	-47	-175
5	-71	-30	-175
6	-83	-20	178

Photophysical studies. The steady state absorption and emission properties of one of the target molecule, BDP-C_{60}-peptide **6**, have been investigated in respect to the parent BDP-C_{60} dyad **1** in order to evaluate the overall photophysical features of the assembly when the helical hexapeptide is linked to the dyad. In addition, the photoinduced processes of this target assembly **6** was studied by transient absorption spectroscopy for the same purpose prior to the immobilization of this family of molecules on gold surfaces. The normalized steady-state absorption and emission spectra of compound **6** in benzonitrile (PhCN) revealed the same trend observed in the parent dyad **1**. The intense absorption bands, located at 330 and 527 nm, are undoubtedly assigned to the methanofullerene and the S_0-S_1 transition of the BDP, respectively (Figure 4). In addition, when compound **6** was excited at 510 nm in PhCN (selective excitation of the BDP), the emission band of the BDP moiety at 535 nm was found to be quenched by over 95 %, which is in analogy with the behavior obtained for the dyad **1**.[10a] These results confirm the insignificant influence of the hexapeptide on the photophysical properties of the target assembly **6**.

10.1002/cplu.202300717

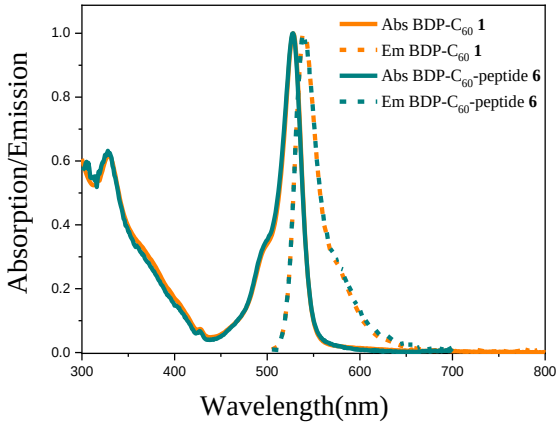

Figure 4. Normalized absorption (solid lines) and emission spectra (dotted lines, λ_{exc} = 510 nm) of BDP-C_{60} dyad **1** (orange) and BDP-C_{60}-peptide **6** (dark cyan) recorded in PhCN.

Femtosecond (fs) transient absorption (TA) spectroscopy was also conducted on the target assembly **6** in a probed spectral range of 330 to 1400 nm (Figure 5). The spectra were recorded in PhCN with selective excitation of the BDP unit using a 527 nm excitation pulse. Identical temporal windows used for the parent BDP-C_{60} dyad **1** were chosen for the sake of comparison. The evolution of the transient species appeared to be very similar to that of the parent dyad **1**.[10a] The transient spectra of assembly **6** identically indicate the presence of both the radical anion $C_{60}^{\bullet-}$ and the excited state $^1C_{60}$* resulting from the photoinduced electron and energy transfer processes, respectively, from the excited BDP to the C_{60} moiety. Furthermore, signatures for singlet excited ^{1}BDP* at 344, 427 and 1280 nm along with ground state bleaching of BDP were noticeable at long delay times up to 2700 ps. This can be attributed to the presence of free-BDP, generated from the rupture of the thiol-maleimide linkage, which is in accordance with the results reported for the parent BDP-C_{60} dyad **1**. [10a]

10.1002/cplu.202300717

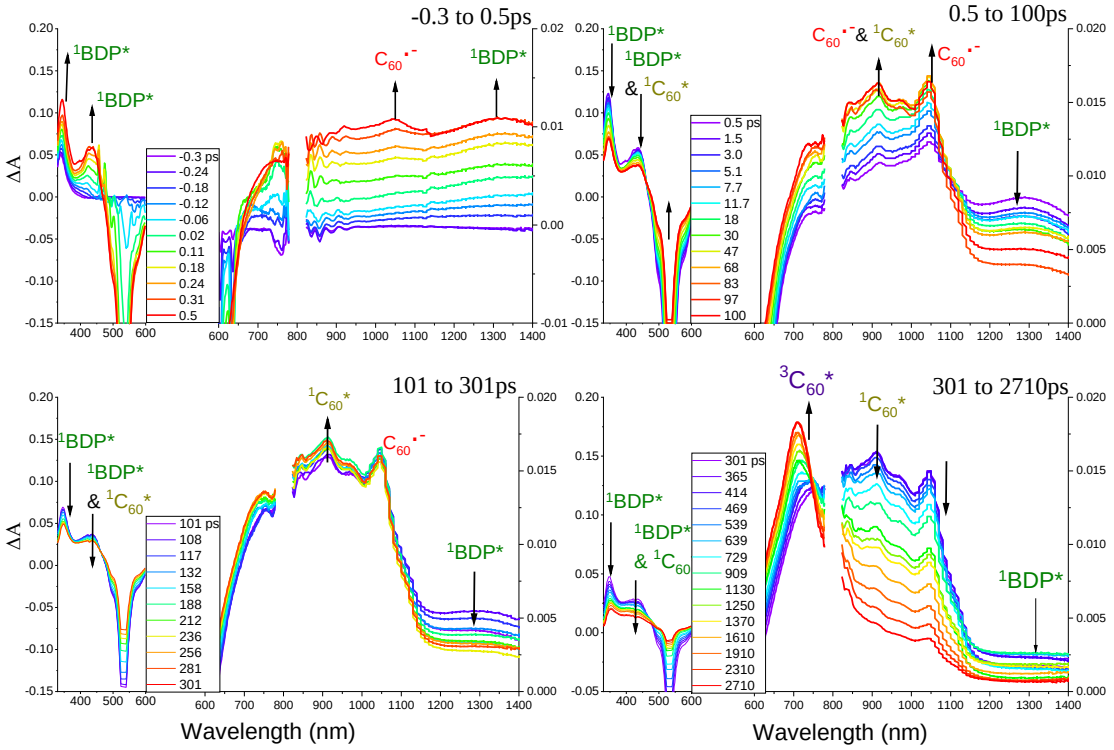

Figure 5. Femtosecond transient absorption spectra of **6** at specified delay times: a) -0.3 to 0.5 ps; b) 0.5 to 100 ps; c) 101 to 301 ps and d) 301 to 2710 ps in PhCN. λ_{exc} = 527 nm.

Furthermore, the kinetic traces of **6** were compared to those of the parent dyad **1** in order to confirm the above-mentioned trend. The superimposed kinetic traces of both compounds at specific probe wavelengths corresponding to the absorption of different intermediates formed upon excitation are provided in Figure S34. It can be clearly seen that the parent BDP-C_{60} dyad **1** and the target assembly **6** seem to follow matching kinetics, indicating a similar relaxation dynamic for the two compounds. The same covalent linker between the BDP donor and C_{60} acceptor in both compounds leads to similar photoinduced electron and energy transfer from BDP to C_{60}. Therefore, these findings confirm the negligible contribution of the helical hexapeptide on the ultrafast dynamics of the overall assembly in solution. The hexapeptide chain introduced on the other side of the fullerene unit acts as an electron mediator between the dyad and the gold surface.

Self-assembled monolayer formation and characterization

The BDP-C_{60}-peptide **6**, BDP-C_{60}-peptide **8** and reference molecules (peptide **4** and C_{60}-peptide **10**) were self-assembled on gold surfaces by exposing a gold coated glass substrate to a solution of the molecules in dichloromethane. The resulting SAMs were firstly investigated using PM-

IRRAS to confirm their composition and to investigate the conformation and orientation of the peptide-based molecules on gold surfaces.

PM-IRRAS. Figure 6 shows representative spectra of the SAMs formed by the molecular assemblies (**4**, **6**, **8** and **10**). Amide I and amide II bands appeared around 1658 and 1542 cm^{-1}, respectively, in all the peptide assemblies (see Table 2) confirming that the helical conformation is retained in the SAMs. These results are in accordance with those obtained in our previous study,[11a] and with helical peptide-based SAMs reported in the literature.[6f, 17]

Additional bands that are characteristic of the functional groups in the target molecules are also observed in the PM-IRRAS SAMs spectra. The C=O of the malonate in the SAMs containing C_{60} groups (*i.e.* BDP-C_{60}-peptide **6**, BDP-C_{60}-peptide **8** and C_{60}-peptide **10**) appeared around 1740 cm^{-1}. In addition, a band characteristic of C=O of the maleimide functions present in BDP-C_{60}-peptide **6** and C_{60}-peptide **10** appeared at 1699 cm^{-1}. These findings confirm the adsorption of the molecular assemblies on the gold surfaces (see Table S1).

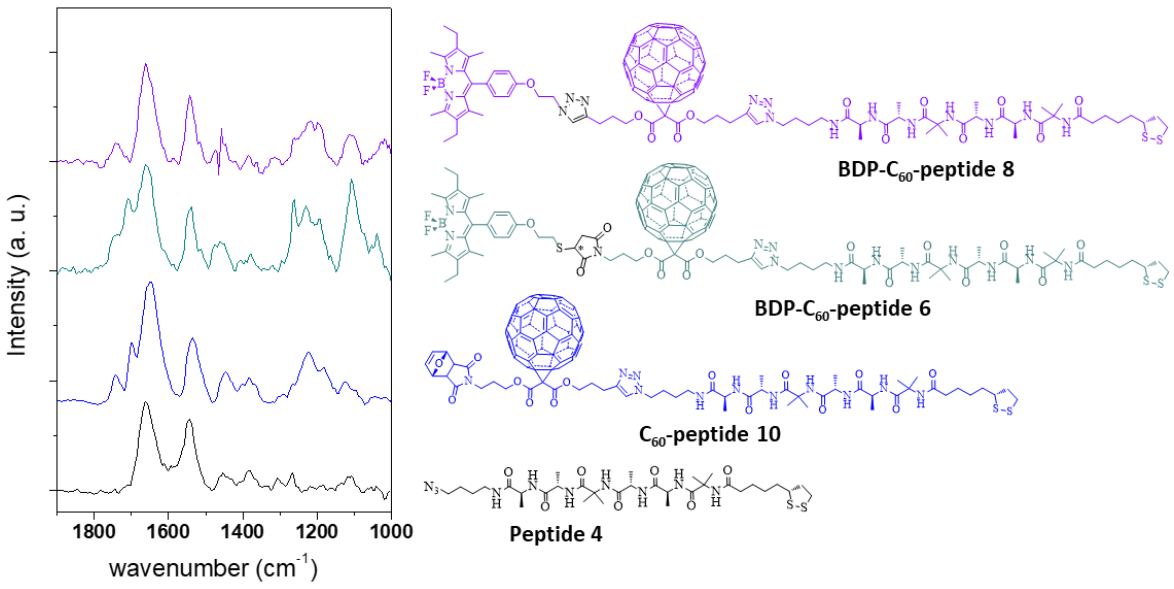

Figure 6. PM-IRRAS spectra of the SAMs grown by peptide **4** (black), C_{60}-peptide **10** (blue), BDP-C_{60}-peptide **6** (green) and BDP-C_{60}-peptide **8** (violet) assemblies and corresponding structures.

Table 2. Amide I and II wavenumbers determined by PM-IRRAS and tilt angles of the helical peptide calculated from the IRRAS data for peptide **4**, C_{60}-peptide **10**, BDP-C_{60}-peptide **6** and BDP-C_{60}-peptide **8** adsorbed on gold.

Compound	Peptide **4** [33]	C_{60}-peptide **10** [33]	BDP-C_{60}-peptide **6**	BDP-C_{60}-peptide **8**
Amide I (cm^{-1})	1658	1658	1659	1661
Amide II (cm^{-1})	1542	1542	1542	1542
Tilt angle γ (deg)	48±3	37±2	40±3	44±2

The tilt angles (γ) of the peptide-based assemblies in the different SAMs on gold surfaces were estimated from the ratio of the amide I and II absorbances.[11a] As pointed out in our previous article, the SAMs formed by the C_{60}-peptide are more vertically oriented with a tilt angle value of 37 (±2°) for **10** in comparison with tilt angles values of 48 (±3°) for the parent peptide **4** and other short peptides described in the literature (49-63° for octapeptides).[2, 18] This was explained by the strong fullerene-fullerene and peptide-peptide intermolecular interactions, resulting in the formation of densely packed monolayers. The tilt angles of the helices from the surface normal in the BDP-C_{60}-peptide **6** and BDP-C_{60}-peptide **8**, were estimated to be 40 (±3) and 44 (±2°), respectively. From these findings, C_{60}-C_{60} interactions in addition to the (expected) peptide-peptide interactions are considered to still be present in BDP-C_{60}-peptide SAMs, leading to a more vertical orientation compared to the peptide alone, but probably to a lesser extent compared to the C_{60}-peptide.

Blocking properties of the SAMs. As in our previous study, a first assessment of the density of SAMs formed with peptide and alkyl chains was assessed by recording cyclic voltammograms (CVs) of $Fe(CN)_6^{3-}$ on modified and unmodified electrodes, as shown in Figure 7.[11a] A significant difference between the responses for the naked gold and modified gold electrodes was observed. In the case of bare gold, a good electrical communication was established resulting in a reversible CV of the ferricyanide/ferrocyanide redox signals. However, in the case of the modified electrodes, these redox signals were strongly attenuated showing that the electron transfer between the redox probe and the electrode was blocked by the SAM formed on the gold surface.

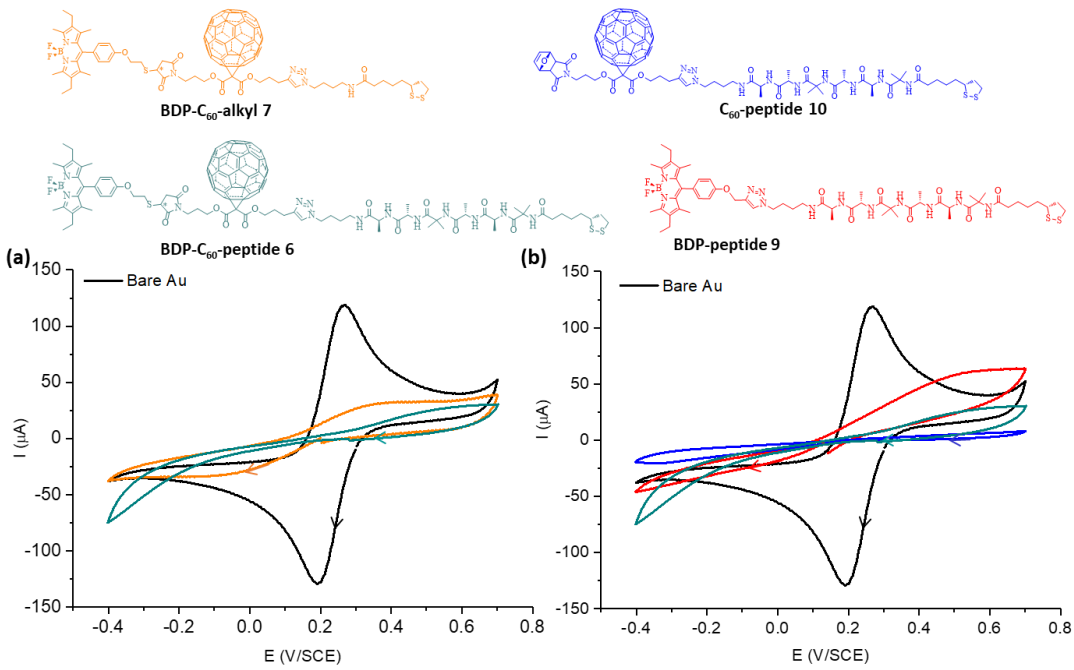

Figure 7. Chemical structures of molecules and CVs experiments in $K_3[Fe(CN)_6]$ (1 mM + 1 M KCl) aqueous solution. Scan rate: 100 mV/s. (a) bare gold electrode and gold electrode modified by the BDP-C_{60}-peptide **6** (green) and BDP-C_{60}-alkyl **7** (orange) SAMs. (b) bare gold electrode and gold electrode modified by the BDP-C_{60}-peptide **6** (green), C_{60}-peptide **10** (blue) and BDP-peptide **9** (red)**.**

First, as expected from our previous work, the Au electrode coated with the SAM formed by BDP-C_{60}-peptide **6** showed a larger decrease in the redox probe signal when compared to the one coated with the BDP-C_{60}-alkyl **7** SAM analog (Figure 7a) showing the contribution of the helical peptide to the density of C_{60} based SAMs.[11a] Secondly, Figure 7b shows that the probe response at the electrode functionalized with the BDP-C_{60}-peptide **6** SAM is slightly higher than the one coated with the C_{60}-peptide **10** SAM. This could be assigned to the disruption of the organization within the monolayer when the BODIPY chromophore was added to the assembly, resulting in a slightly less dense monolayer. These findings are consistent with those obtained from the estimation of tilt angles by PM-IRRAS. Finally, the SAM formed by the BDP-peptide **9** derivative allowed an increase in the electroactive probe signal compared to C_{60}-peptide **10** and BDP-C_{60}-peptide **6** SAMs (Figure 7b). This can be associated with the absence of fullerenes, which help organization within the SAM by their C_{60}-C_{60} interactions, in addition to less steric hindrance of the BODIPY unit compared to the fullerene unit.

Ultra-fast electrochemistry. In order to confirm that our hybrid molecules are strongly adsorbed on gold and to show that their redox properties are conserved, the CV of the different SAMs were performed on a gold ball microelectrode. This powerful technique, which, to our knowledge, has never been used to investigate peptide-based SAMs, provides access both to

surface coverage and electron transfer (ET) rate constants. High scan rates in the range 100-20000 $V{\cdot}s^{-1}$ were used to avoid any chemical reaction consecutive to electron transfer as observed with other C_{60} molecules.[19] Interestingly, all the recorded CVs of the SAMs formed by our family of molecules at different scan rates exhibited well-resolved signals with a bell-shape behavior, and peak currents proportional to the scan rate (see Figure S37) as expected for adsorbed systems.

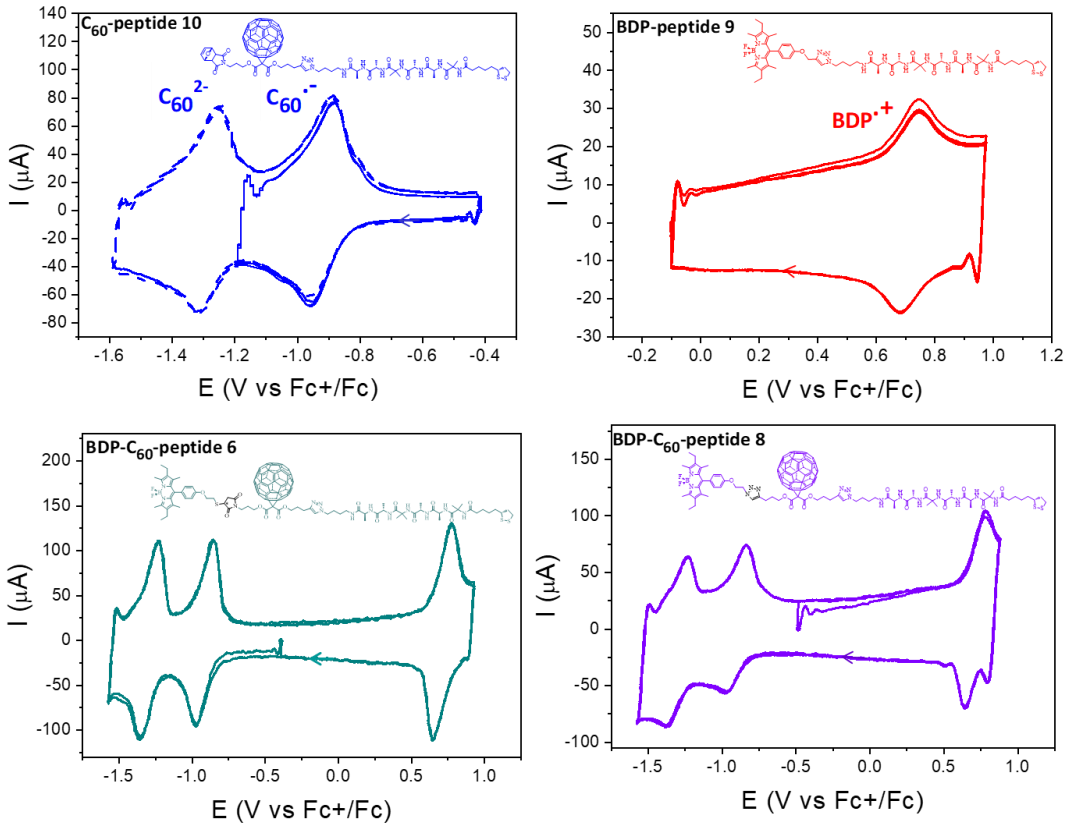

Figure 8. CVs of C_{60}-peptide **10** (blue) at 4800 $V{\cdot}s^{-1}$, BDP-peptide **9** (red) at 4400 $V{\cdot}s^{-1}$, BDP-C_{60}-peptide **6** (green) at 5100 $V{\cdot}s^{-1}$and BDP-C_{60}-peptide **8** (violet) at 10000 $V{\cdot}s^{-1}$ adsorbed on a gold microelectrode and corresponding structures. Electrolyte: DCM + *n*-Bu_4PF_6 (0.3M).

General electrochemical investigations were firstly carried out on the SAMs formed by the reference molecules C_{60}-peptide **10** and BDP-peptide **9**. The recorded cyclic voltammograms are displayed in Figure 8 and their half-wave potentials *vs.* ferrocene used as reference are summarized in Table 3. The CV of C_{60}-peptide **10** immobilized on a gold microelectrode displayed reversible and well resolved peaks with bell-shape behavior corresponding to the first and second one-electron reduction waves of C_{60} at standard potentials of -0.92 V and -1.28 V (*vs.* Fc^+/Fc), as already observed for several other C_{60} immobilized systems. The CV recorded on the SAM formed by BDP-peptide **9** on a gold microelectrode exhibited a reversible well-

resolved peak at +0.72 V (*vs.* Fc^+/Fc) corresponding to the oxidation of the BODIPY entity. The peak-to-peak separations in the low scan rate regime are respectively 20 and 18 mV for C_{60} and BDP. These values are close to the ideal electrochemically reversible behavior (0 mV).

The CVs of the SAMs formed by BDP-C_{60}-peptide **6** and BDP-C_{60}-peptide **8** are shown in Figure 8. Both CVs exhibited stable and well-defined reversible redox waves with a bell-shape behavior that can be roughly explained by the sum of C_{60}-peptide (reduction of the C_{60} core) and BDP-peptide (oxidation of the BODIPY unit) which implies weak electronic coupling between both redox entities in the ground state. In addition, the obtained half-wave redox potentials of the assembled monolayers formed by BDP-C_{60}-peptide **6** and BDP-C_{60}-peptide **8** on a gold microelectrode are very similar (see Table 3) suggesting that the nature of the linker connecting the two electro-active moieties (thiol-maleimide or triazole) has no significant effect on the electronic properties of the SAMs. Integration of the area under the cathodic or anodic peak, owing to the first/second reductions of the C_{60} and the oxidation of the BODIPY, respectively, allowed us to calculate the surface coverage of our target and reference assemblies on the gold microelectrodes. This method is extremely useful for our study since it provides important information regarding the density of the molecules' assemblies on gold surfaces. The estimated surface coverage values Γ ($mol{\cdot}cm^{-2}$) and the calculated electron transfer rate constant (s^{-1}) of our target and reference assemblies on gold microelectrodes are listed in Table 3.

Table 3. Electrochemical Half-Wave Potentials (V vs Fc+/Fc) of C_{60}-peptide **10**, BDP-peptide **9**, BDP-C_{60}-alkyl **7**, BDP-C_{60}-peptide **6** and **8** and the estimated surface coverage values Γ ($mol{\cdot}cm^{-2}$) and the calculated electron transfer rate constant (s^{-1}).

Compounds		C_{60}-peptide **10**	BDP-peptide **9**	BDP-C_{60}-alkyl **7**	BDP-C_{60}-peptide **6**	BDP-C_{60}-peptide **8**
Potential (V *vs.* Fc^+/Fc)	$BDP^{0/+}$	-	+0.71	+0.71	+0.71	+0.71
	$C_{60}^{0/-}$	-0.92	-	-0.91	-0.91	-0.89
	$C_{60}^{-/2-}$	-1.28	-	-1.29	-1.29	-1.29
Surface coverage Γ (10^{-11} $mol{\cdot}cm^{-2}$)		6.50±0.65[a]	1.95±0.20[b]	1.77±0.18[a]	3.07±0.31[b]	2.15±0.22[b]
Electron transfer rate constant k_S (10^4 s^{-1})		8.0	8.0	3.8	5.0 (C_{60}) 5.0 (BDP)	5.5 (C_{60}) 5.0 (BDP)

[a] Integration of the area under the first C_{60} reduction peak; [b] Integration of the area under the BDP oxidation peak

Beginning with the reference assemblies C_{60}-peptide **10** and BDP-peptide **9**, the estimated surface coverage was found to be around 6.50×10^{-11} and 1.95×10^{-11} mol·cm^{-2}, respectively. This indicates that the SAMs grown by the former assembly are more densely packed than those formed by the latter molecule, which is in accordance with the blocking effect experiments described above. The threefold higher density for the C_{60}-peptide assembly is undoubtedly attributed to the cooperative effect of the fullerene and peptide manifested by intermolecular interactions between the assemblies (C_{60}-C_{60} and helix-helix interactions) that forces a vertical tendency of the monolayers on the gold substrate, resulting in a better surface coverage.

On the other hand, the calculated surface coverage of BDP-C_{60}-peptide **6** and BDP-C_{60}-peptide **8**, estimated at around 3.07×10^{-11} and 2.15×10^{-11} mol·cm^{-2} respectively, appeared to be lower than that corresponding to the C_{60}-peptide **10** assembly and slightly higher than the one corresponding to BDP-peptide **9**. Again, this result confirmed the tilt angles obtained by PM-IRRAS and blocking effect results which show that the additional BODIPY entity on the assemblies might slightly disrupt organization within the monolayers. These experimental surface coverages were compared to calculated ones and found to be in good agreement (see Figures S38-S42 in the SI).

At all scan rates the C_{60} and BDP peaks are well-resolved, indicating a narrow distribution both of standard potentials and rate constants, with low electrostatic interactions between the electroactive moieties.[20] These results are thus again in agreement with well-ordered monolayers. From the peak potential evolution with the scan rate, we could extract the electron transfer rate constants between the electroactive centers and the electrode that are reported in Table 3. The detailed procedure is described in the SI. Interestingly, the obtained values are in the same range from 3.8×10^{4} up to 8×10^{4} s^{-1}. Electron transfer rate constant k_S values are influenced by several parameters.[21] The first is the reorganization energy within and in the proximity of the redox entity. Even for the same redox center, it may vary slightly depending on solvation, which depends on its position within the monolayer, in a bent conformation or fully in solution. The second is the electronic coupling. It typically presents an exponential decrease with the distance between the electrode and the redox entity, until the intervention of electron hopping that dampens this dependence over large distances. In peptides, the transition between tunneling and hopping has been debated. Upon coil formation, H-bonds favor electronic communication so that distance dependence is attenuated compared to alkyl systems but is overall still exponential.[22] Electron hopping, thus creating intermediate redox states in the peptide chain, has been shown to allow propagation and communication over distances as long as 10 nm.[2, 12a] In our case, it is interesting to note concerning C_{60} that k_S is larger for the

peptide assemblies in comparison to the alkyl derivative while the distance between C_{60} and the surface is longer in the peptide than in the alkyl systems (see Figure S43), and that the largest value is reported for the higher coverage. In our former work dealing with C_{60} fullerodendrimers, we reported k_S values as high as 2×10^5 s^{-1}.[23] These results were explained by folding of the molecule to come within a close distance of the electrode, thus favoring electronic coupling. One plausible explanation is that, in our systems, the large k_S values observed for C_{60} reduction does not stem from peptide folding but rather from improved tunneling through the rigid H-bond network as already suggested by Maran et al.[22] In contrast, we suggest that the flexibility of the BDP linker allows an approach close enough to the electrode so that k_S is also large for the BDP oxidation.

Thus, ultrafast electrochemistry demonstrates that electronic communication towards the electrode is efficient, which is important for extracting electrons during photoelectrochemical experiments.

Photoelectrochemistry. Photoelectrochemical measurements were conducted on the SAMs prepared from BDP-C_{60}-peptide **6**, C_{60}-peptide **10**, BDP-C_{60}-alkyl **7** and BDP-C_{60}-peptide **8** in order to investigate their potential in converting the resulting excited states and/or charge-separated state after photo-illumination of the BODIPY-C_{60} part[10, 24] into electrical energy (photocurrent generation) through a vectorial electron relay. The photoelectrochemical measurements of the SAMs were carried out in an argon saturated Na_2SO_4 solution (0.1 M) containing ascorbic acid (AsA) (0.05 M) as a sacrificial electron donor.

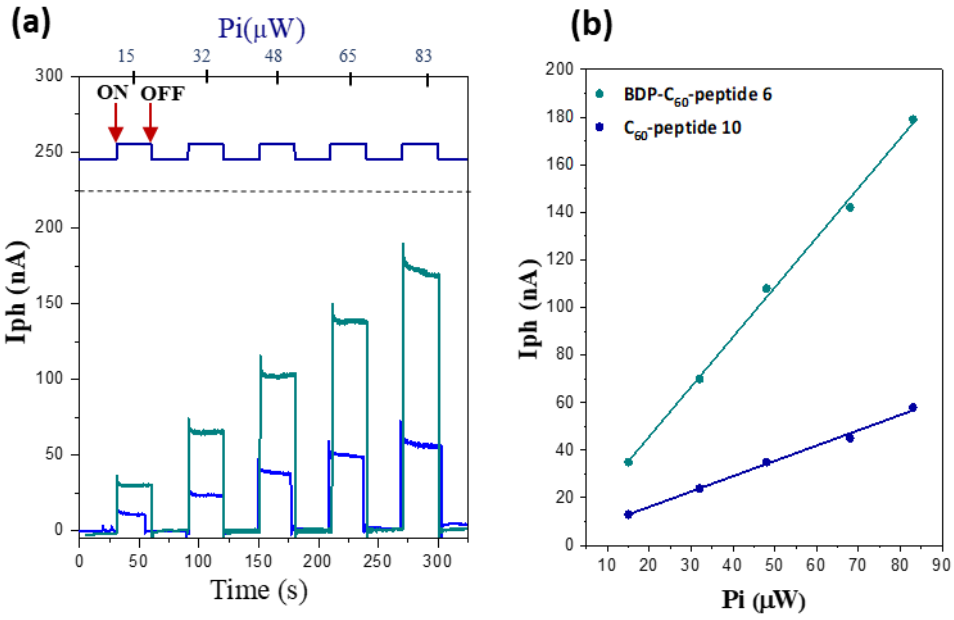

Figure 9. (a) Photoelectrochemical response of BDP-C_{60}-peptide **6** (green) and C_{60}-peptide **10** (blue) SAMs modified Au electrode at V_{OC} with a light intensity variation (λ = 367 nm), in AcA 0.05M + Na_2SO_4 0.1M aqueous solution; **(b)** Linear dependency of photocurrent on Pi of BDP-C_{60}-peptide **6** and C_{60}-peptide **10** SAMs modified electrode.

We investigated first the photoelectrochemical response of the SAM formed by the reference assembly C_{60}-peptide **10** and BDP-C_{60}-peptide **6**, by irradiating at 367 nm, where the C_{60} entity mainly absorbs.[10a] As shown in Figure 9, anodic photocurrent with linear behavior depending on the LED power intensity from 15 to 83 μW was observed. Interestingly, when the SAM formed with BDP-C_{60}-peptide **6** was irradiated at 367 nm, a 2-3 times higher photocurrent intensity was observed in comparison with the SAM constituted of assembly C_{60}-peptide **10** despite the 2.1 times higher surface coverage of the SAM formed by the latter assembly (Table 3). Actually the ratio between the photocurrent intensities normalized to surface coverage is 4-6. This enhancement could be attributed to an additional *intramolecular* photoinduced event that occurs from the BODIPY to the excited states of C_{60} in **6**, generating a charge separated state in comparison to the only *intermolecular* transfer from the external electron carrier (AsA) to the triplet excited state of C_{60} (nearly unit quantum yield of formation) in **10** (*vide infra*).

Moving forward, we decided to switch the excitation wavelength to 550 nm where the BODIPY entity selectively absorbs in order to increase visible-photon harvesting in the photo-current generation cells based on the different SAMs. As expected, the electrode modified by the SAM of reference assembly C_{60}-peptide **10** displayed no photocurrent response due to the negligible absorption of fullerene at this wavelength. Furthermore, a similar observation was obtained in the "fullerene free" SAM-modified electrode derived from reference molecule BDP-peptide **9**. This could be associated with the absence of a long-lived triplet excited state in the case of the BDP chromophore which does not enable efficient intermolecular electron transfer from the AsA as observed for C_{60}-peptide **10**.

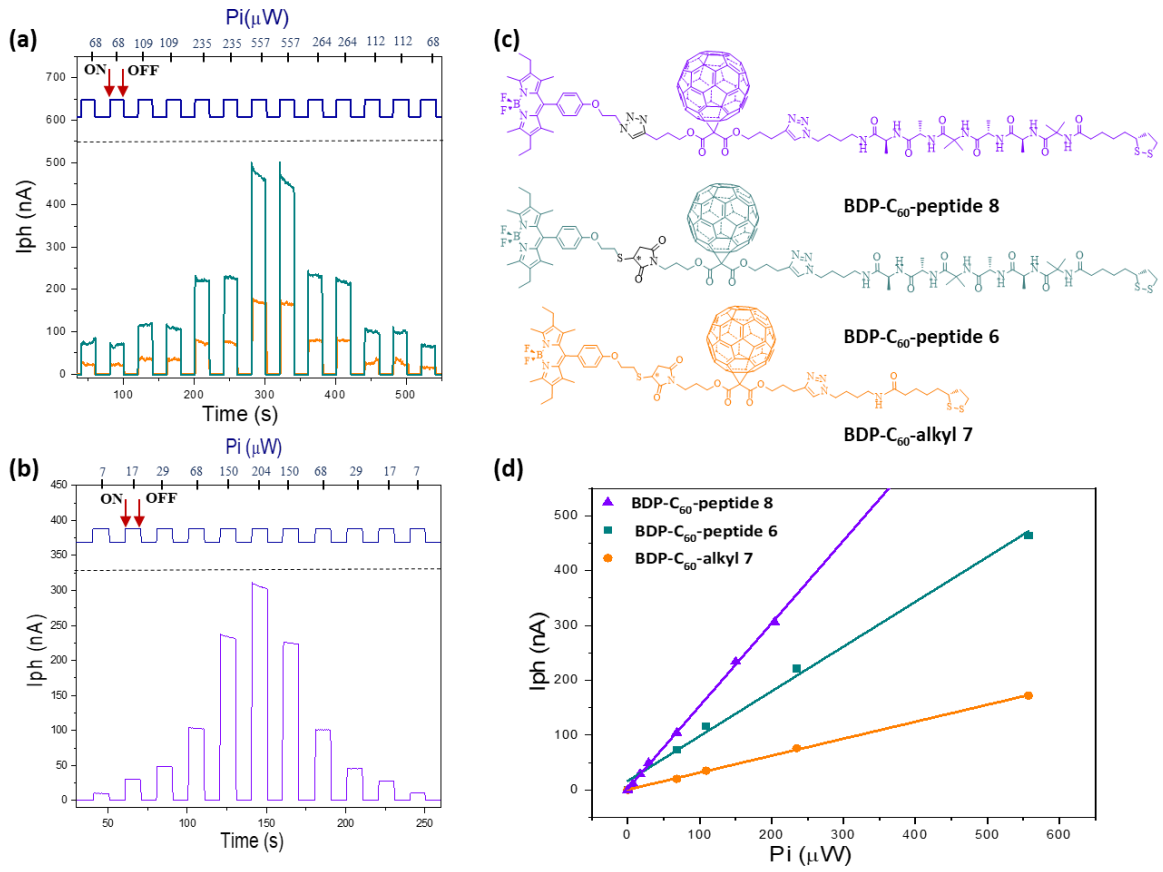

Figure 10. (a) Photoelectrochemical responses of BDP-C_{60}-peptide **6** (green) and BDP-C_{60}-alkyl **7** (orange) SAM modified electrodes at V_{OC} with light intensity variation (λ = 550 nm); **(b)** Photoelectrochemical response of BDP-C_{60}-peptide **8** SAM modified electrode at V_{OC} with light intensity variation (λ = 550 nm) and **(c)** the corresponding molecular structures **(d)** Linear dependency of photocurrent on Pi of BDP-C_{60}-peptide **6**, BDP-C_{60}-alkyl **7** and BDP-C_{60}-peptide **8** SAM modified electrodes.

Regarding BDP-C_{60}-peptide **6** SAMs, irradiated at 550 nm, a photocurrent response was obtained that increased linearly with the light power Pi from 68 to 557 μW. The opposite behavior was detected in a similar linear trend when the light intensity was decreased (Figure 10a). Moreover, the photoelectrochemical response of BDP-C_{60}-peptide **6** SAM was compared to that generated by its alkyl chain analog BDP-C_{60}-alkyl **7** SAM (Figure 10a and 10d). The generated photocurrent response by this latter assembly was found to be lower than that produced by the BDP-C_{60}-peptide **6**. For a given Pi, the intensity observed for BDP-C_{60}-alkyl **7** SAM was 2-3 times lower than that observed for BDP-C_{60}-peptide **6** SAM. The lower photocurrent response in the alkyl based SAM could be explained by the interplay of three factors: (1) the higher surface density of peptide based SAM in comparison with alkyl SAM, which implies more photoactive BDP-C_{60} species for the generation of anodic photocurrent (Table 3, surface coverage ratio of compounds **6**/**7** is 1.7); (2) the better electron mediating properties and faster electron transfer kinetics through helical peptides in comparison with alkyl

chains observed by ultrafast electrochemistry; (3) the higher quenching of the BODIPY singlet excited state in the dyad by energy transfer to the gold electrode in the case of flexible and loosely packed monolayers formed by the alkyl chains.

Finally, when the target molecule BDP-C_{60}-peptide **8** SAM was irradiated at the same wavelength, a photocurrent response was generated that was higher (1.5 times, for the highest Pi tested) compared to the photocurrent obtained for the BDP-C_{60}-peptide **6** SAM assembly (Figure 10b and 10d). This could be attributed to the higher stability of the triazole linker connecting the BODIPY entity to the fullerene in the BDP-C_{60}-peptide **8** assembly. Whereas in the case of BDP-C_{60}-peptide **6**, detachment of BDP due to the breaking of the thiol-maleimide linkage, as observed in ultra-fast electrochemistry experiments in the case of alkyl derivative **7** (See SI, Figure S36), could prevent efficient charge/energy transfer between the fullerene and the photo-excited state of BDP, resulting finally in a lower photocurrent response.

As pointed out in our previous studies, both energy and electron transfer processes have been demonstrated in the BDP-C_{60} dyads **1** and **2** in solution. [10, 24] Similar photoinduced events were also illustrated in the BDP-C_{60}-peptide **6** (see Photophysical studies). Thus, the same processes could be expected in BDP-C_{60}-peptide SAMs. On the basis of these findings and previous work reported in the literature,[25] we can propose two different photocurrent generation mechanisms as illustrated in Figure 11. The photoexcitation of the BODIPY entity within these assemblies generates the singlet excited state ^{1}BDP*, which undergoes a fast energy transfer and electron transfer processes to the C_{60}, yielding the singlet excited state $^1C_{60}$* and radical anion $C_{60}^{\bullet-}$ species, respectively. The latter specie directly gives an electron to the gold surface through the helical hexapeptide bridge (or alkyl chain) by an intramolecular ET process while the electron sacrificer (AsA) gives an electron to the BODIPY radical cation to regenerate the neutral form (Figure 11c). In this case, the vectorial anodic electron flow occurs from AsA to the gold through the charge separated BDP-C_{60} state. Concurrently, the photo-generated $^1C_{60}$* specie yields the $^3C_{60}$* through intersystem crossing (ISC) that extracts an electron from the electron sacrificer AsA, leading again to the formation of $C_{60}^{\bullet-}$, which subsequently gives its electron to the gold surface, and thus generates an anodic photocurrent response (Figure 11b). Again, the vectorial anodic electron flow occurs from AsA to the gold but this time through the excited triplet state of the C_{60}. In both cases, the rate-determining step should be the electron transfer from the $C_{60}^{\bullet-}$ anion radical to the gold surface since the ET from AsA to the triplet excited state of C_{60} or to the BDP cation radical should be very fast due

to the high concentration of AsA (50 mM) and to their close location at the interface between the water and the SAM.

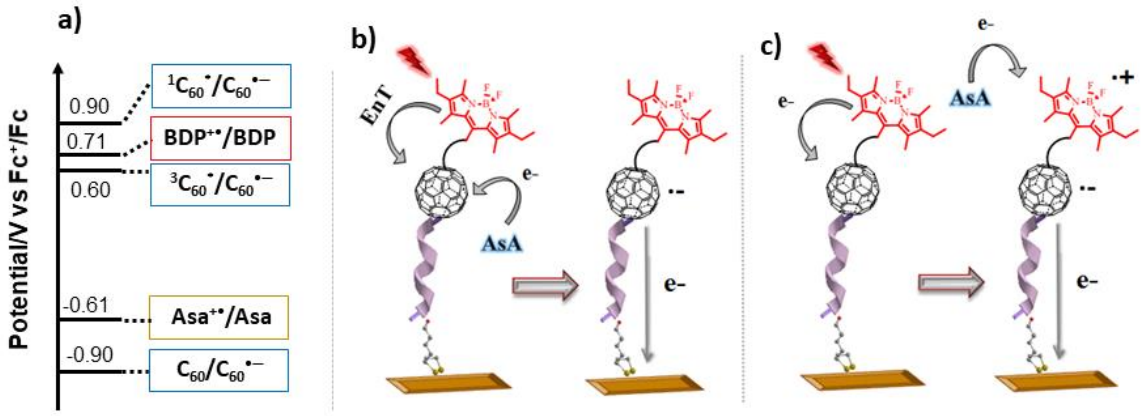

Figure 11. a) Diagram showing the redox potentials of C_{60}, $^{1}C_{60}$*, $^{3}C_{60}$*, BDP and AsA, redox potentials of C_{60} excited states are estimated by taking into consideration the redox potential of fullerene derivatives/Au measured in DCM (see Table 3) and the excitation energy[26]; **b, c)** Schematic mechanisms of the anodic photocurrent generated by **6** and **8**-SAM.

Conclusion

In summary, we describe in this work the synthesis and characterization of two novel BDP-C_{60}-peptide assemblies, as well as references molecules, that were immobilized on gold surfaces through the formation of SAMs. The complete characterization of the SAMs formed by these assemblies, using a combination of surface analyses and cyclic voltammetry, allowed us to draw solid conclusions regarding their conformation, composition, and organization within the monolayers. The estimation of the surface densities and calculation of tilt angles, using CV (blocking effect and **Γ**) and PM-IRRAS showed that the peptide-based SAMs BDP-C_{60}-peptide **6** and **8** are more densely packed than their alkyl analog BDP-C_{60}-alkyl **7**. This was attributed to the rigid peptide helical conformation, as well as peptide-peptide and C_{60}-C_{60} interactions. These results are in accordance with those previously obtained for the C_{60}-peptide **10** and C_{60}-alkyl **11**. However, less dense monolayers were obtained in the case of the target assemblies BDP-C_{60}-peptide when compared to the C_{60}-peptide. This can be attributed to the presence of the BODIPY entity that may disrupt organization within the monolayers.

Regarding the ET kinetics, the estimated values of the electron transfer constants determined by ultra-fast electrochemistry were found to be faster in the case of the peptide-based monolayers than their alkyl-based analogs despite a more dense and rigid assembly and thus longer average distance between the electrode and C_{60} unit, which confirms the ability of the helical peptide to act as a better electron mediator in comparison with alkyl chains.

Finally, photoelectrochemical systems containing our target BDP-C_{60}-peptides assemblies have revealed a better photocurrent response in comparison with that generated by the systems formed by the reference molecules (containing alkyl chains or lacking one of the primary redox centers). The presence of the C_{60} entity within the photoelectrochemical systems is vital for the generation of photocurrent, which again confirms that C_{60} is an excellent electron mediator in PET processes, owing to its small reorganization energy and electron accepting properties. In addition, the contribution of the helical peptide, not only as a surface structuring agent but also as a good electron mediator, is highly beneficial for the generation of a higher photocurrent response in comparison with the alkyl-based analog SAMs. Finally, the presence of the BODIPY chromophore entity is also indispensable due to its visible light harvesting and electron donor properties.

Based on these findings, we have confirmed the valuable contribution of peptide-based SAMs by combining short helical peptides with BODIPY-C_{60} dyads for the development of organic light-to-current conversion in molecular devices.

Supporting Information

The authors have cited additional references within the Supporting Information.[27] The Supporting Information includes the synthesis and characterization of compounds **6**-**9**. The NMR and Mass spectra of these compounds are depicted in Figures S3-S33. The experimental details for photophysical studies, for SAM formation and characterization are described in the SI. The superimposed kinetic traces of compounds **1** and **6**, and absorption and emission spectra of BDP-peptide **9** are depicted in Figures S34 and S35, respectively. The CVs of **7** in solution and adsorbed on a gold microelectrode are depicted in Figure S36. The CVs of the target (**6** and **8**) and reference assemblies (**7**, **9** and **10**) SAMs on gold microelectrode at different scan rates are provided in Figure S37. Finally, the calculated surface coverages of compounds **6** to **10** are given in Figures S38-S42.

Acknowledgements

This work was supported by the LabEx CHARMMMAT ANR-11-LABX-0039 and PALM ANR-10LABX-0039-PALM, by the CNRS (International Emerging Action, PICS project no 08198), Région Ile-de-France DIM NanoK, the University of Versailles St-Quentin-en-Yvelines and University of Paris-Saclay. J. Rabah thanks the MESRI « Ministère de l'Enseignement Supérieur de la Recherche et de l'Innovation » for a PhD fellowship (2017-2020).

Keywords: Fullerene C60 • Boron dipyrromethene • Peptides • Monolayers • Electron transfer

Entry for the Table of Contents

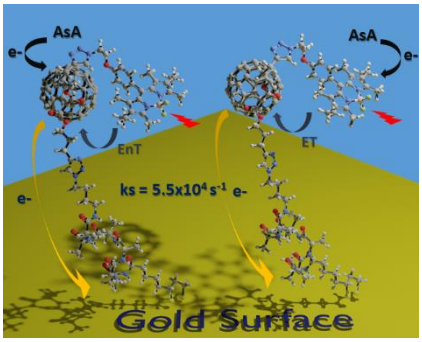

BODIPY-C_{60}-helical peptide constructs could form densely packed self-assembled monolayers (SAMs) on gold surfaces. Ultra-fast electrochemistry experiments showed the helical peptide was a better electron mediator compared to an alkyl chain. This property was exploited along with those of the BODIPY-C_{60} dyads for photo-current generation by converting the resulting excited and/or charge separated states produced by photo-illumination into electrical energy.

Institute and/or researcher Twitter usernames: Institut Lavoisier Versailles @ILV_UMR8180

References

[1] a) A. Shah, B. Adhikari, S. Martic, A. Munir, S. Shahzad, K. Ahmad and H. B. Kraatz, *Chemical Society Reviews* **2015**, *44*, 1015-1027; b) N. Amdursky, *ChemPlusChem* **2015**, *80*, 1075-1095.
[2] Y. Arikuma, H. Nakayama, T. Morita and S. Kimura, *Angewandte Chemie - International Edition* **2010**, *49*, 1800-1804.
[3] S. Kimura, *Organic & biomolecular chemistry* **2008**, *6*, 1143-1148.
[4] a) S. Yasutomi, T. Morita, Y. Imanishi and S. Kimura, *Science* **2004**, *304*, 1944-1947; b) K. Kitagawa, T. Morita and S. Kimura, *Angewandte Chemie International Edition* **2005**, *44*, 6330-6333.
[5] a) E. Gatto and M. Venanzi, *Israel Journal of Chemistry* **2015**, *55*, 671-681; b) E. Gatto, R. Lettieri, L. Vesce and M. Venanzi, *Energies* **2022**, *15*, 5632.
[6] a) T. Morita, K. Yanagisawa and S. Kimura, *Polymer Journal* **2008**, *40*, 700-709; b) E. Gatto, L. Stella, F. Formaggio, C. Toniolo, L. Lorenzelli and M. Venanzi, *Journal of Peptide Science* **2008**, *14*, 184-191; c) R. Moritoh, T. Morita and S. Kimura, *Biopolymers* **2013**, *100*, 1-13; d) E. Gatto, A. Quatela, M. Caruso, R. Tagliaferro, M. De Zotti, F. Formaggio, C. Toniolo, A. Di Carlo and M. Venanzi, *ChemPhysChem* **2014**, *15*, 64-68; e) M. Venanzi, E. Gatto, M. Caruso, A. Porchetta, F. Formaggio and C. Toniolo, *The Journal of Physical Chemistry A* **2014**, *118*, 6674-6684; f) H. Uji, Y. Yatsunami and S. Kimura, *The Journal of Physical Chemistry C* **2015**, *119*, 8054-8061; g) H. Uji, K. Tanaka and S. Kimura, *Journal of Physical Chemistry C* **2016**, *120*, 3684-3689; h) E. Gatto, S. Kubitzky, M. Schriever, S. Cesaroni, C. Mazzuca, G. Marafon, M. Venanzi and M. De Zotti, *Angewandte Chemie International Edition* **2019**, *58*, 7308-7312; i) S. Kubitzky, M. Venanzi, B. Biondi, R. Lettieri, M. De Zotti and E. Gatto, *Chemistry – A European Journal* **2021**, *27*, 2810-2817.
[7] a) H. Imahori, Y. Mori and Y. Matano, *Journal of Photochemistry and Photobiology C: Photochemistry Reviews* **2003**, *4*, 51-83; b) H. Yamada, H. Imahori, Y. Nishimura, I. Yamazaki, T. K. Ahn, S. K. Kim, D. Kim and S. Fukuzumi, *Journal of the American Chemical Society* **2003**, *125*, 9129-9139.
[8] a) D. M. Guldi, G. M. A. Rahman, V. Sgobba and C. Ehli, *Chemical Society Reviews* **2006**, *35*, 471; b) E. Espíldora, J. L. Delgado and N. Martín, *Israel Journal of Chemistry* **2014**, *54*, 429-439; c) S. Fukuzumi, K. Ohkubo and T. Suenobu, *Accounts of Chemical Research* **2014**, *47*, 1455-1464; d) M. Rudolf, S. V. Kirner and D. M. Guldi, *Chemical Society Reviews* **2016**, *45*, 612-630; e) O. Ito, *The Chemical Record* **2017**, *17*, 326-362; f) G. Bottari, G. de la Torre, D. M. Guldi and T. Torres, *Coordination Chemistry Reviews* **2021**, *428*, 213605; g) C. Müller, S. Bold, M. Chavarot-Kerlidou and B. Dietzek-Ivanšić, *Coordination Chemistry Reviews* **2022**, *472*, 214764.
[9] a) H. Imahori and S. Fukuzumi, *Advanced Functional Materials* **2004**, *14*, 525-536; b) D. Bonifazi, O. Enger and F. Diederich, *Chem. Soc. Rev.* **2007**, *36*, 390-414; c) G. V. Dubacheva, C.-K. Liang and D. M. Bassani, *Coordination Chemistry Reviews* **2012**, *256*, 2628-2639.
[10] a) T.-T. Tran, J. Rabah, M.-H. Ha-Thi, E. Allard, S. Nizinski, G. Burdzinski, S. Aloïse, H. Fensterbank, K. Baczko, H. Nasrallah, A. Vallée, G. Clavier, F. Miomandre, T. Pino and R. Méallet-Renault, *The Journal of Physical Chemistry B* **2020**, *124*, 9396-9410; b) A. Fatima, J. Rabah, E. Allard, H. Fensterbank, K. Wright, G. Burdzinski, F. Miomandre, J. Pham, G. Clavier, M. Sliwa, T. Pino, R. Méallet-Renault, K. Steenkeste and M. H. Ha-Thi, *The European Physical Journal Special Topics* **2022**.
[11] a) H. Nasrallah, J. Rabah, V. Bui-Thi-Tuyet, K. Baczko, H. Fensterbank, F. Bourdreux, A. M. Goncalves, V. Declerck, S. Boujday, V. Humblot, K. Wright, A. Vallée and E. Allard, *New Journal of Chemistry* **2018**, *42*, 19423-19432; b) J. Rabah, L. Yonkeu, K. Wright, A. Vallée, R. Méallet-Renault, M.-H. Ha-Thi, A. Fatima, G. Clavier, H. Fensterbank and E. Allard, *Tetrahedron* **2021**, *100*, 132467.
[12] a) B. Giese, M. Napp, O. Jacques, H. Boudebous, A. M. Taylor and J. Wirz, *Angewandte Chemie International Edition* **2005**, *44*, 4073-4075; b) C. Zuliani, F. Formaggio, L. Scipionato, C. Toniolo, S. Antonello and F. Maran, *ChemElectroChem* **2020**, *7*, 1225-1237.
[13] a) K. Baczko, H. Fensterbank, B. Berini, N. Bordage, G. Clavier, R. Méallet-Renault, C. Larpent and E. Allard, *Journal of Polymer Science Part A: Polymer Chemistry* **2016**, *54*, 115-126; b) H. Fensterbank, K. Baczko, C. Constant, N. Idttalbe, F. Bourdreux, A. Vallée, A.-M. Goncalves, R. Méallet-Renault, G. Clavier, K. Wright and E. Allard, *The Journal of Organic Chemistry* **2016**, *81*, 8222-8233.

[14] A. Polese, S. Mondini, A. Bianco, C. Toniolo, G. Scorrano, D. M. Guldi and M. Maggini, *Journal of the American Chemical Society* **1999**, *121*, 3446-3452.
[15] a) S. Carlotto, P. Cimino, M. Zerbetto, L. Franco, C. Corvaja, M. Crisma, F. Formaggio, C. Toniolo, A. Polimeno and V. Barone, *Journal of the American Chemical Society* **2007**, *129*, 11248-11258; b) A. Moretto, M. Crisma, F. Formaggio, B. Kaptein, Q. B. Broxterman, T. A. Keiderling and C. Toniolo, *Peptide Science: Original Research on Biomolecules* **2007**, *88*, 233–238; c) A. Moretto, F. Formaggio, B. Kaptein, Q. B. Broxterman, L. Wu, T. A. Keiderling and C. Toniolo, *Biopolymers* **2008**, *90*, 567-574; d) C. Tonlolo and E. Benedetti, *Trends in Biochemical Sciences* **1991**, *16*, 350-353.
[16] in *Deposition number 2309195 contains the supplementary crystallographic data for this paper. These data are provided free of charge by the joint Cambridge Crystallographic Data Centre and Fachinformationszentrum Karlsruhe Access Structures service*, *Vol.*
[17] K. Yanagisawa, T. Morita and S. Kimura, *Journal of the American Chemical Society* **2004**, *126*, 12780-12781.
[18] M. Kai, K. Takeda, T. Morita and S. Kimura, *Journal of peptide science* **2008**, 192-202.
[19] a) L. Le-Quang, R. Farran, Y. Lattach, H. Bonnet, H. Jamet, L. Guérente, E. Maisonhaute and J. Chauvin, *Langmuir* **2018**, *34*, 5193-5203; b) P. Fortgang, E. Maisonhaute, C. Amatore, B. Delavaux-Nicot, J. Iehl and J. F. Nierengarten, *Angewandte Chemie - International Edition* **2011**, *50*, 2364-2367; c) P. Fortgang, M. Urbani, M. Holler, J. F. Nierengarten, A. Moreau, B. Delavaux-Nicot and E. Maisonhaute, *Electroanalysis* **2015**, *27*, 1010-1016.
[20] G. Boitel-Aullen, L. Fillaud, F. Huet, I. Nierengarten, B. Delavaux-Nicot, J. F. Nierengarten and E. Maisonhaute, *ChemElectroChem* **2021**, *8*, 3506-3511.
[21] X. S. Zhou, B. W. Mao, C. Amatore, R. G. Compton, J. L. Marignier, M. Mostafavi, J. F. Nierengarten and E. Maisonhaute, *Chemical Communications* **2016**, *52*, 251-263.
[22] S. Antonello, F. Formaggio, A. Moretto, C. Toniolo and F. Maran, *Journal of the American Chemical Society* **2003**, *125*, 2874-2875.
[23] J. A. Camerano, M. A. Casado, U. Hahn, J. F. Nierengarten, E. Maisonhaute and C. Amatore, *New Journal of Chemistry* **2007**, *31*, 1395-1399.
[24] A. Fatima, J. Rabah, E. Allard, H. Fensterbank, K. Wright, G. Burdzinski, G. Clavier, M. Sliwa, T. Pino, R. Méallet-Renault, K. Steenkeste and M.-H. Ha-Thi, *Photochemical & Photobiological Sciences* **2022**, *21*, 1573-1584.
[25] H. Imahori, T. Azuma, A. Ajavakom, H. Norieda, H. Yamada and Y. Sakata, *The Journal of Physical Chemistry B* **1999**, *103*, 7233–7237.
[26] D. M. Guldi and M. Prato, *Accounts of Chemical Research* **2000**, *33*, 695-703.
[27] a) L. Liang, J. Ruiz and D. Astruc, *Advanced Synthesis & Catalysis* **2011**, *353*, 3434-3450; b) A. Vallée, V. Humblot, R. Al Housseiny, S. Boujday and C.-M. Pradier, *Colloids and Surfaces B: Biointerfaces* **2013**, *109*, 136-142; c) Y. Miura, S. Kimura, Y. Imanishi and J. Umemura, *Langmuir* **1998**, *14*, 6935-6940; d) M. Tsubio, *Journal of Polymer Science* **1962**, *59*, 139-153; e) C. Amatore, E. Maisonhaute, B. Schöllhorn and J. Wadhawan, *ChemPhysChem* **2007**, *8*, 1321-1329; f) A. J. Bard and L. R. Faulkner, *Electrochemical Methods: Fundamentals and Applications*, Wiley India Ltd.: New Delhi, **2004**, p; g) Y. Wang, E. I. Rogers and R. G. Compton, *Journal of Electroanalytical Chemistry* **2010**, *648*, 15-19; h) Y. Shirai, L. Cheng, B. Chen and J. M. Tour, *Journal of the American Chemical Society* **2006**, *128*, 13479-13489.